Microporous and Mesoporous Materials 288 (2019) 109555

Contents lists available at ScienceDirect

Microporous and Mesoporous Materials

journal homepage: www.elsevier.com/locate/micromeso

Structural investigation of interlayer-expanded zeolite by hyperpolarized ^{129}Xe and ^{1}H NMR spectroscopy

Zhenchao Zhao[a,b,1], Xin Li[c,1], Shihan Li[a], Shutao Xu[b,*], Xinhe Bao[b], Yilmaz Bilge[d], Parvulescu Andrei-Nicolae[d], Müller Ulrich[d], Weiping Zhang[a,**]

[a] State Key Laboratory of Fine Chemicals, School of Chemical Engineering, Dalian University of Technology, Dalian, 116024, China
[b] State Key Laboratory of Catalysis, Dalian Institute of Chemical Physics, Chinese Academy of Sciences, 457 Zhongshan Road, Dalian, 116023, China
[c] College of Chemistry and Chemical Engineering, Henan University of Technology, Zhengzhou, 450001, China
[d] BASF SE, Process Research and Chemical Engineering, 67056, Ludwigshafen, Germany

ARTICLE INFO

Keywords:
Layered zeolite
Interlayer expanding
Pore structure
^{129}Xe NMR
Silanol group

ABSTRACT

The interlayer expanded zeolite COE-4 was synthesized using silylation agents such as dichlorodimethylsilane (DCDMS) as layer linker from layered silicate RUB-36 precursor. Solid-state NMR techniques combined with theoretical calculations have proven to be a useful characterization method to investigate the structure and porosity of the interlayer expanded zeolites. XRD and ^{29}Si MAS NMR results show that after calcination the layer spacing of COE-4 is enlarged by 2.6 Å compared with that of RUB-37, indicating that pore windows between the layers are enlarged from 8-membered ring (8-MR) pores to 10-MR pores due to the formation of $Si(OH)_2$ pillar between adjacent layers. Hyperpolarized (HP) ^{129}Xe NMR results indicate that after interlayer expansion, Xe atoms can be adsorbed in the 10-MR channels of COE-4, and the 10-MR channels are homogeneously distributed like ZSM-5. For COE-4, Xe has a stronger interaction with the channel walls containing dual silanol groups. ^{1}H MAS NMR combined with theoretical calculations make a clear assignment of dual silanol groups at 3.3 ppm, and the concentration of dual silanols is 2.2 mmol/g, which is 1–2 orders of magnitude larger than the concentration of the other two types of existing isolated and hydrogen-bonded silanol groups. After introduction of pyridine-d_5, one Si–OH from the dual silanol groups has a weak hydrogen bond interaction with pyridine molecule, and the adsorbed pyridine molecule may experience chemical exchange with the other Si–OH of the dual silanol group and therefore ^{1}H NMR signal of dual silanol groups shows a weak broad peak at 5.7 ppm after pyridine adsorption.

1. Introduction

Zeolites are a class of crystalline microporous aluminosilicates with three dimensional (3D) framework structures widely used as shape-selective catalysts, ion exchangers, and adsorbents [1,2]. The shape-selectivity arises from its distinct distribution of active sites and topological structure. Therefore, synthesis of zeolites with new topological structures are highly desirable [3]. Generally, zeolites are synthesized directly from inorganic precursors assembled in the presence of organic/inorganic structure-directing agents (SDAs) to form ordered crystalline material [4,5]. In most cases, 3D zeolites are formed, but some layered zeolite precursors (LZPs) can also be formed [6,7]. These layered zeolite precursors are composed from the layer unit of the parent 3D zeolite and the layers are stacked by weak interactions such as hydrogen bond or charge interactions [7,8]. During a high temperature treatment (calcination) process, the silanol groups of adjacent layers will start to condense to form a 3D structure if they have closely fitted distance [8]. In fact, some zeolites with new topological structures such as CDO, RRO, OKO, PCR etc. can only be obtained from their LZPs [6,9–11]. Moreover, many approaches have been proposed to expand the corresponding zeolite derivatives based on LZPs, such as swelling, pillaring, delamination, intercalation, and even a new concept "assembling, disassembling, organizing, reorganizing (ADOR)" have been developed [6,9,12,13]. These modifications can even finely tune the interlayer pore size/shape and improve the accessibility of the active sites resulting both of an expansion in zeolite properties and their

* Corresponding author.
** Corresponding author.
E-mail addresses: xushutao@dicp.ac.cn (S. Xu), wpzhang@dlut.edu.cn (W. Zhang).
[1] Z.Z. and X.L. contributed equally to this work.

https://doi.org/10.1016/j.micromeso.2019.06.017
Received 15 April 2019; Received in revised form 30 May 2019; Accepted 14 June 2019
Available online 18 June 2019
1387-1811/

catalytic applications. For example, Wu et al. first synthesized interlayer expanded zeolite MWW (IEZ-MWW) via orderly pillaring the adjacent MWW layers by a silicon atom [14]. The silicon pillar was introduced by condensation reaction between an alkoxysilane and two silanol groups of adjacent MWW layers in layered MWW precursors. After calcination, the methyl groups turned into dual silanol groups and therefore IEZ-MWW has 12-MR pores. In comparison with conventional 10-MR Ti-MWW zeolite, Ti-containing IEZ-MWW catalyst showed much higher conversion and specific activity in cyclohexene oxidation with H_2O_2. Similarly, Xiao et al. successfully synthesized a novel crystalline microporous titanosilicate (Ti-COE-4) with functionalized hydroxyl groups and medium micropore size (0.55 nm) from Ti-RUB-36. The synergism of silanol groups with active Ti sites in Ti-COE-4 significantly improves its catalytic performance in oxidation reactions [15]. Intensive studies on interlayer expanded zeolites RUB-36 and RUB-39 were conducted including thiol group functionalized silicon and heteroatoms such as Sn、Ti、Fe、Al etc. used as pillars. The obtained catalysts showed distinct catalytic activities in olefin epoxidation, alkane catalytic cracking/isomerization and biomass conversion reactions [16–23].

Interlayer expansion has proven to be a very successful approach to obtain new classes of layered zeolite derivatives from their LZPs with precisely controlled pore geometries equivalent to conventionally directly made zeolites. The new formed structures are mainly determined by X-ray diffractions and HRTEM combined with Rietveld refinement [18,24]. However, the homogeneity of pillaring and the structure of defect silanol or dual silanol groups between the layers haven't been systematically studied while these defects/silanol groups may have significant impact on the shape-selective effect or the activity of active centers in catalysis [15,25]. Herein, we report a convenient and effective method to determine the order of the interlayer structure of IEZ-CDO (COE-4) using HP ^{129}Xe NMR spectroscopy. Xenon atom is very sensitive to the pore size and the interaction with other guest molecules in a restricted geometry [26]. The use of optical pumping techniques for the production of HP xenon can increase sensitivity of several orders of magnitude ($\times 10^4$). It has been shown that HP ^{129}Xe NMR technique is very powerful in studying the porosity of porous materials [26–32], or even the reaction processes and kinetics [33–35]. On the other hand, ^{1}H MAS NMR spectroscopy was also utilized to investigate the acidity of the silanol groups in the interlayer combined with adsorption of d5-pyridine probe molecule. Density functional theory (DFT) calculations were also conducted to interpretate the interaction between xenon atoms as well as pyridine and silanol groups.

2. Experimental Section

2.1. Synthesis of COE-4

Layered silicate RUB-36 was synthesized following our previous report using Aerosil 200 as the silica source and diethyldimethylammonium hydroxide as the structure-directing agent (DEDMAOH, 20 wt% solution in water, Sachem Inc.) [36]. The interlayer expansion reaction was carried out according to the following procedures. Typically, 0.9 g of dichlorodimethylsilane (DCDMS) was added into 150 ml of HCl solution (0.7 M), followed by addition of 3.0 g of pure silica RUB-36. After stirring for 4 h and ultrasonic treatment for 2 h at room temperature, the sample was transferred into an autoclave for the treatment at 180 °C for 24 h. After filtration and drying, 2.7 g of solid product, designated as COE-3, was obtained. After calcination at 550 °C for 6 h, the organic groups in COE-3 were completely removed, yielding a new material, which was designated as COE-4.

2.2. Characterization

XRD patterns were collected on a Rigaku D/Max-RB diffractometer using Cu $K\alpha$ radiation with a range of 2θ value from 5° to 50° and a scanning rate of 5°/min.

Solid-state NMR spectra were recorded on a Varian Infinityplus-400 spectrometer. ^{29}Si MAS and ^{1}H→^{29}Si CP/MAS NMR spectra were acquired at 79.4 MHz using a 5 mm MAS probe with a spinning rate of 6 kHz. The chemical shifts were referenced to 4,4-dimethyl-4-silapentane sulfonate sodium (DSS) at 0 ppm. Before ^{1}H MAS NMR measurements, the samples were dehydrated at 400 °C under a vacuum below 10^{-2} Pa for 20 h. Pyridine-d_5 molecules were adsorbed on samples at room temperature for 20 min, and then the sealed samples were heated to 300 °C for 15 h treatment to make the pyridine full contact with samples. After the treatment, the samples were evacuated under vacuum at 50 °C for desorption of physical adsorbed pyridine molecules. ^{1}H MAS NMR spectra were collected at 399.9 MHz using a csecho sequence with a $\pi/4$ pulse, a 4 s recycle delay, and a spinning speed of 10 kHz. The chemical shifts were referenced to adamantane at 1.74 ppm. For quantitative analysis, all the samples were weighed, and the spectra were calibrated by measuring a known amount of 1,1,1,3,3,3-hexafluoro-2-propanol performed in the same acquisition conditions [37]. The Dmfit software was used for deconvolution using Gaussian-Lorentzian line shapes [38].

Continuous-flow HP ^{129}Xe NMR spectra were collected at 110 MHz under static conditions. Optical polarization of xenon was achieved with a home-built pumping cell in the fringe field of the spectrometer magnet and a 60 W dual diode laser array (Coherent Inc.). A flow of 1% Xe, 1% N_2 and 98% He gas mixture was delivered to the sample region via plastic tubing. Variable temperature measurements were performed from room temperature to 173 K. All of the spectra were acquired with a 3.0 μs $\pi/4$ pulse, 100–200 scans, and a 2 s recycle delay. The chemical shifts were referenced to the signal of xenon gas.

2.3. Theoretical calculation method

For Xe adsorption, two typical cluster models including a 10-membered ring with/without silanol groups, and models including straight channel/intersections were derived from the crystal structure of COE-4 and MFI, respectively [18,39]. Each peripheral Si atom was saturated with hydrogen atoms at a Si–H distance of 1.5 Å orienting along the bond direction to the next lattice oxygen atom. All the Si–H bond were kept fixed at their crystallographic locations with other atoms relaxed during the structure optimization. The structure optimizations were performed within generalized gradient approximation (GGA) at PW91 correlation functionals and DNP basis set as implemented in DMol3 [40,41]. The NMR parameters were calculated by the GIAO method and performed on the Gaussian09, Revision D01program package [42]. Density functional theory with the B3LYP hybrid functional method and standard DZVP basis sets for Xe, 6-31G (d,p) for other atoms were employed [43,44]. For qualitative comparison, relativistic effects and dynamics of Xe were not taken into account here for ^{129}Xe chemical shift calculation, which may affect the accuracy of calculated values [45,46]. The ^{129}Xe NMR chemical shift was reported in ppm relative to the free Xe atom. Counterpoise (CP) correction is applied to reduce the basis set superposition error (BSSE) [47], which is important not only for interaction energies but also for molecular electronic properties.

^{1}H NMR chemical shift calculations were also conducted using the Gaussian09 program package. A cluster model with a center dual silanol group extending 4T sites was taken from COE-4 [18], and the dangling bonds were saturated with hydrogen atoms pointing to the next oxygen atom of experimental unit cell. Geometry optimization was performed using ONIOM method by DFT/B3LYP, which is proved to be feasible in many zeolite-related systems [48–51]. 6-31G (d,p) and 3-21G basis set with D3 + BJ dispersion correction were employed for high-level and low-level layers, respectively [52,53]. All the NMR parameters were calculated by the GIAO method. ^{1}H chemical shifts are simulated at the B3LYP/pcs-1 level using fully optimized tetramethylsilane (TMS) as a reference to convert the calculated isotropic

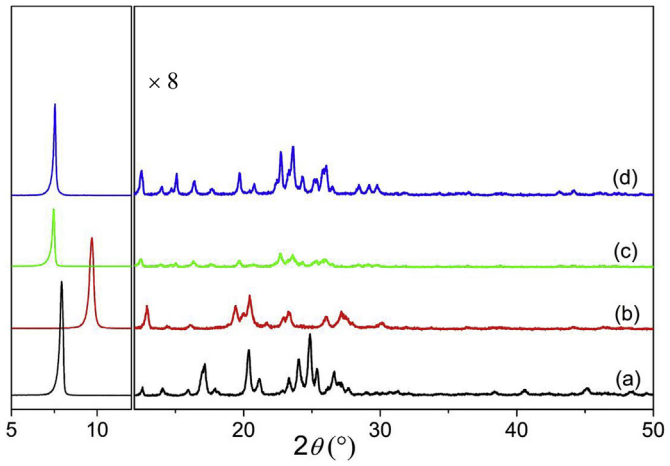

Fig. 1. XRD patterns of RUB-36 (a), calcined RUB-36 (CDO, RUB-37) (b), precursor of IEZ-CDO (COE-3) (c), and calcined COE-3 (COE-4) (d). The patterns of scattering angle 2θ over 12° are enlarged by 8 times.

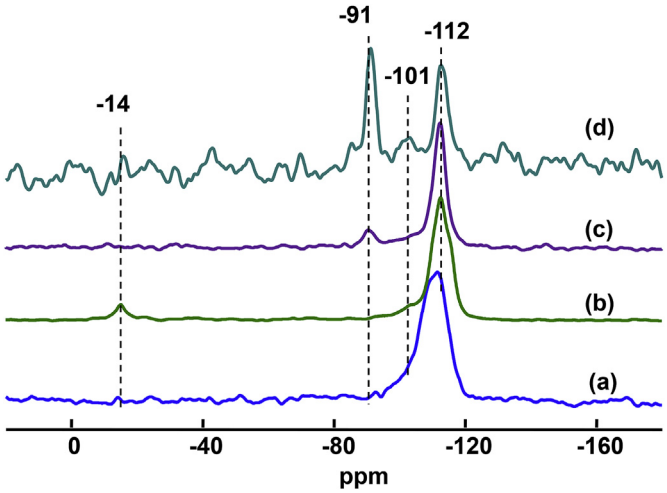

Fig. 2. ^{29}Si MAS NMR spectra of RUB-37 (a), COE-3 (b), COE-4 (c) and ^{1}H→^{29}Si CP/MAS NMR spectrum of COE-4 (d).

absolute shielding constants.

3. Results and discussion

3.1. XRD and ^{29}Si MAS NMR

Fig. 1 shows powder XRD patterns of the precursor RUB-36, RUB-37 (CDO) and IEZ-CDO samples. All XRD patterns show strong characteristic peaks of layer-related diffractions with 2θ near 8°. RUB-36 is composed of FER layers stacking in translation symmetry with DEDMA intercalated between the layers. After calcination of RUB-36, the adjacent 2D layers link into the 3D CDO structure (RUB-37) with interlayer windows of dual 8-MR pores (along [001] and [010] directions) through the condensation of the silanol groups on the layer surface. As a result, the layer-related diffraction peak shifts from 2θ = 7.92° (d = 11.15 Å) to 9.69° (d = 9.12 Å). However, for IEZ-CDO samples (COE-3 and COE-4), the diffraction peak associated with the layers shifts to a lower scattering angle (2θ = 7.54°, d = 11.72 Å) in comparison with RUB-36 and RUB-37 because of the silylation with Me_2SiCl_2 species, implying that the insertion of $Me_2Si=$ species leads to the expansion of the interlayer space. The layer space of COE-4 is enlarged by 2.6 Å compared with that of RUB-37, which is in accordance with the fact that pore windows between the layers are enlarged from 8-MR to 10-MR pores.

The ^{29}Si MAS NMR spectra of RUB-37, COE-3 and COE-4 zeolites are shown in Fig. 2. The signals at −112 ppm, −101 ppm and −91 ppm are assigned to $Si(OSi)_4$ (Q^4), $Si(OH)(OSi)_3$ (Q^3) and $Si(OH)_2(OSi)_2$ (Q^2) groups, respectively [54]. For RUB-37, there are mainly Q^4 and Q^3 groups shown in Fig. 2a. Whereas, for COE-3 (Fig. 2b), there is another peak at −14 ppm, which can be assigned to the Si–CH_3 species [55]. The results indicate that the silylation occurred through the reaction of DCDMS with the silanols on the layer surface to form pillaring silicon species between the layers. After calcination, the peak at −14 ppm disappears, indicating that the methyl groups turn into the OH groups to form Q^2 sites connected to the adjacent layers in COE-4 (Fig. 2c). It is consistent with the ^{1}H→^{29}Si CP/MAS NMR spectrum (Fig. 2d), that shows the signal intensity of Q^2 group was significantly enhanced.

3.2. Investigation of interlayer porosity with HP ^{129}Xe NMR

The pore sizes of 8-MR along [010] and [001] directions in CDO are 3.1 × 4.7 Å and 2.5 × 4.2 Å, respectively [39]. Therefore, it is difficult for xenon to adsorb in the channels because of the relatively larger dynamic diameter of xenon atom (4.4 Å). HP ^{129}Xe NMR spectra of RUB-37, COE-4 and H-ZSM-5 (Si/Al = 100) zeolite with 10-MR channels for comparison were collected at various temperatures, and the spectra are shown in Fig. S1 and Fig. 3. The peaks at 0 ppm in the spectra are from xenon in the gas phase. All signals at lower field are originated from the adsorbed xenon in the zeolites. For RUB-37 (Fig. S1), a signal of adsorbed xenon appears near 89 ppm at mesopore region below 233 K and the chemical shifts of the line moved to lower field slightly when the temperature further decreased [56,57]. This signal is from the accumulated pores of the zeolite particles but not from the 8-MR channels of RUB-37. For COE-4 (Fig. 3a), the signal of adsorbed xenon at micropore region can be observed at 293 K and the chemical shift of the line increases from 111 to 205 ppm when the temperature is decreased from 293 to 173 K. This is a general trend in variable-temperature ^{129}Xe NMR experiments mainly due to the increase of the Xe–Xe interactions at lower temperatures even if the partial pressure of xenon is quite small [58–60]. However, fast exchange of Xe adsorbed at different sites at higher temperatures and preferable adsorption at certain site of Xe at lower temperatures may also contribute the temperature dependence of chemical shift of ^{129}Xe as is reported by Komulainen et al. [45]. In comparison of RUB-37 and COE-4, HP ^{129}Xe NMR results demonstrate unambiguously the success of interlayer expansion of RUB-36 by DCDMS. Moreover, the signals of adsorbed Xe in the micropores of COE-4 have high symmetry, implying the pillared 10-MR pore sizes have homogeneous distribution. Whereas, variable-temperature HP ^{129}Xe NMR spectra of H-ZSM-5 (Fig. 3b) also show one line ascribed to Xe adsorbed in the 10-MR micropores. The temperature-dependent behavior of the line is similar to COE-4 (Fig. 3c). The chemical shift of adsorbed xenon in the 10-MR channels increases from 106 to 167 ppm when the temperature is decreased from 293 to 173 K. The smaller chemical shift difference (Δδ) between COE-4 and H-ZSM-5 samples at 293 K indicates that the pore sizes of these two samples are very close. But the chemical shift difference increases more obviously as the decrease of temperature.

Theoretical calculations were further conducted to compare Xe adsorption behavior using models including 10-MR derived from part of the crystal structure of COE-4 and ZSM-5. The optimized cluster models are presented in Fig. 4, where the calculated ^{129}Xe NMR chemical shifts are also denoted. As many factors such as the pressure of Xe and temperature can influence the ^{129}Xe NMR chemical shifts, it is difficult to obtain a calculated value that is the same as the experimental one, but it can give a trend for detailed analysis. In fact, there are two typical adsorption sites for Xe in both COE-4 and ZSM-5. As is shown in Fig. 4, Xe can be adsorbed in the channels with (Fig. 4a) and without (Fig. 4b) silanols groups for COE-4, and the calculated chemical shifts are 180.2 and 51.0 ppm, respectively. Similarly, Xe atom can be adsorbed in the

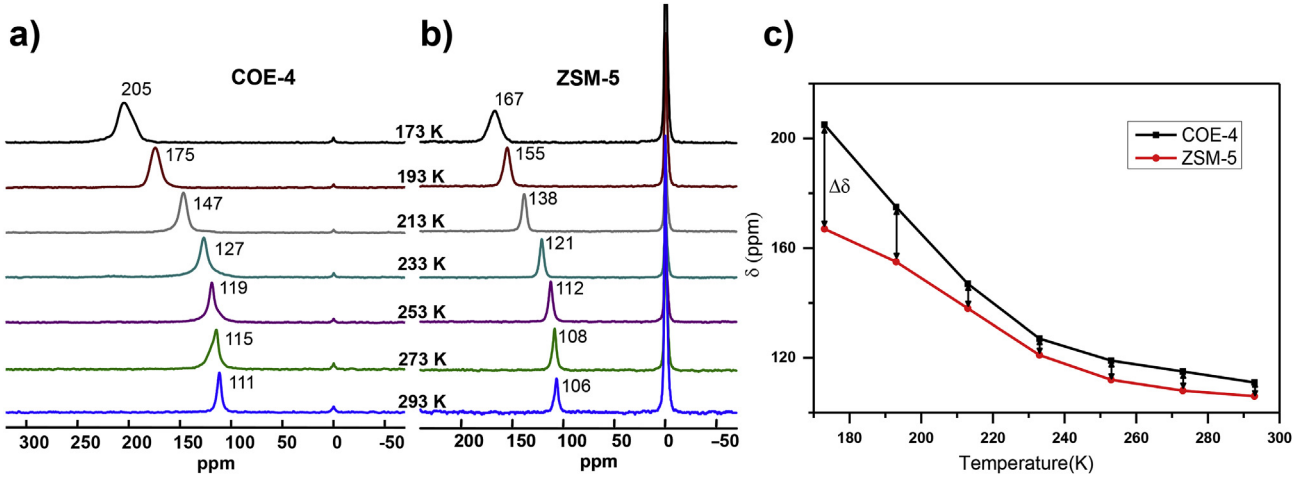

Fig. 3. HP ^{129}Xe NMR spectra of COE-4 (a) and H-ZSM-5 (b) at various temperatures and corresponding temperature-dependence curves of chemical shift (c).

straight channel (Fig. 4c) and intersections (Fig. 4d) for ZSM-5, and the calculated chemical shifts are 118.5 and 58.6 ppm, respectively. The chemical shift of ^{129}Xe adsorbed in channels without silanol groups (Fig. 4b) in COE-4 is very close to that adsorbed in the intersections (Fig. 4d) in ZSM-5. Whereas, ^{129}Xe chemical shift of Xe adsorbed in the channel with silanol groups in COE-4 shifts significantly lower field (180.2 ppm) compared with Xe adsorbed in the straight channel (118.5 ppm) in ZSM-5. Considering the experimental result that ^{129}Xe signal of COE-4 shifts significantly lower field at 173 K, we can infer that Xe may preferably be adsorbed in the channels containing silanol groups in COE-4 at lower temperatures. It means COE-4 has stronger interaction between Xe and 10-MR channel wall than H-ZSM-5 at lower temperature that results in larger chemical shift. At relatively higher temperatures, Xe adsorbed at different sites experience fast exchange as these adsorption sites are cross-connected by 10-MR rings (Fig. S2), and therefore they show very close ^{129}Xe chemical shift.

3.3. ^{1}H MAS NMR investigation of interlayer acidity with Pyridine-d_5

Deuterated pyridine (pyridine-d_5) is one of the widely used NMR probe molecules for acidic detection [61,62]. The formation of a hydrogen bond between pyridine and non-acidic hydroxyl groups (such as Si–OH) generally shifts the ^{1}H MAS NMR signal from 2 to about 10 ppm. The ^{1}H MAS NMR spectra of RUB-37 and COE-4 zeolites before and after pyridine-d_5 adsorption are shown in Fig. 5. The peaks at 1.7 ppm and 2.3/2.7 ppm are assigned to isolated silanol groups and silanol groups with hydrogen bond effect, respectively [63]. The broad peaks centered at 4.5/4.6 ppm belong to residually adsorbed water. For COE-4, there is another dominant peak at 3.3 ppm that is not observed in RUB-37. Therefore, it should be due to dual silanols in the interlayer. Quantitative analysis results of the spectra are shown in Table 1. There is no obvious change of the concentrations of isolated silanol groups and silanol groups with hydrogen bond effect for both samples. But the concentration of dual silanols for COE-4 is 2.2 mmol/g, which is 1–2 orders of magnitude larger than the other two types of silanol groups.

After introduction of pyridine-d_5, ^{1}H MAS NMR spectrum of RUB-37 is unchanged indicating that pyridine is hardly adsorbed into the channels of RUB-37. For COE-4, when pyridine is adsorbed at 300 °C or 400 °C then desorbed at 100 °C, the peak of dual silanols disappeared and a broad weak signal at 5.7 ppm is observed that may be attributed to the hydrogen bond interaction between pyridine and dual silanols. The peaks between 8 and 9 ppm are from the resident H-type pyridine molecules in pyridine-d5. Therefore, it is another evidence that in COE-4 the FER layers are successfully interlayer expanded by DCDMS. When the desorption temperature is increased to 150 °C, the peak of dual silanols appears again accompanied with the decrease of that of pyridine. This indicates the interaction between pyridine and dual silanols is weak and pyridine is not protonated.

To further confirm above assignments of ^{1}H MAS NMR signals of COE-4 at 3.3 ppm and 5.7 ppm before and after pyridine adsorption, theoretical calculations were conducted. The optimized cluster model of COE-4 before and after pyridine adsorption are shown in Fig. 6. The calculated chemical shift of dual silanol group is 3.1 ppm, which agrees well with the experimental result. After pyridine adsorption, ^{1}H chemical shift of the hydrogen bonded proton is 11.0 ppm with the other ^{1}H atom at 3.3 ppm in the dual silanol group, which is similar to generally observed around 10 ppm chemical shift of silanol groups after adsorption of pyridine [63]. It is reasonable to infer that the adsorbed pyridine molecule may experience chemical exchange with the other silanol group of the dual silanol group. Therefore, the experimental chemical shift of dual silanol groups after pyridine adsorption should lie in the range of 3.3–11.0 ppm, which is in accordance with the

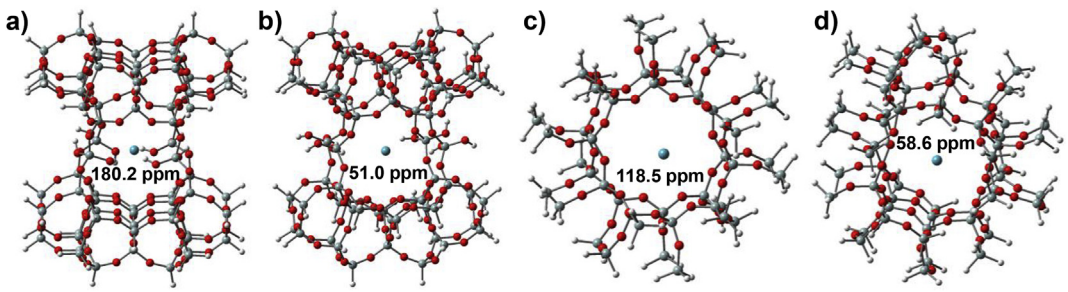

Fig. 4. The optimized models for Xe adsorbed in COE-4 in the channels with (a) and without (b) silanol groups and ZSM-5 in the straight channel (c) and intersection (d) and their corresponding ^{129}Xe NMR chemical shifts. (The cyan ball denotes xenon atom). (For interpretation of the references to colour in this figure legend, the reader is referred to the Web version of this article.)

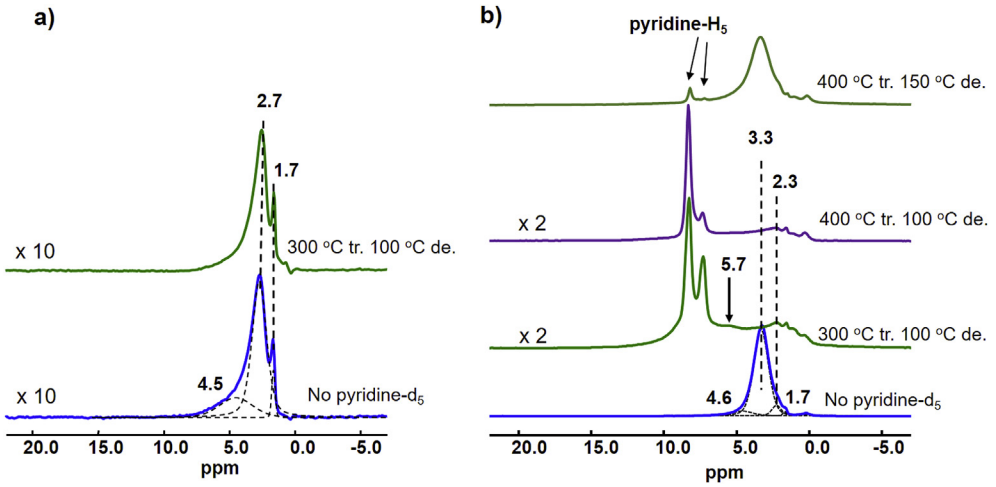

Fig. 5. ^{1}H MAS NMR spectra of (a) RUB-37 and (b) COE-4 zeolites before and after adsorption of deuterated pyridine under different conditions.

Table 1
Concentration of various silanol groups in RUB-37 and COE-4 zeolites.

Sample	1.7 ppm (mmol/g)	2.3/2.7 ppm (mmol/g)	3.3 ppm (mmol/g)
RUB-37	1.7×10^{-2}	2.4×10^{-1}	–
COE-4	2.4×10^{-2}	1.6×10^{-1}	2.2

experimentally observed broad weak signal near 5.7 ppm. This kind of exchange reflects some extent mobility of pyridine molecules in the zeolite channels, and spin-echo NMR experiment can effectively decrease the signal intensity due to fast molecular isotropic reorientation. Therefore, spin-echo NMR experiment was conducted to estimate the mobility of molecules by changing the time interval of two pulses (the pulse sequence was shown in Fig. S3). Fig. 7 shows the ^{1}H spin-echo MAS NMR spectra of COE-4 zeolite after pyridine-d_5 adsorption with different time intervals from 100 μs to 1000 μs, There is an obvious decrease of the signal intensity of the peak at 5.7 ppm when increase the interval from 100 μs to 500 μs, which indicates that the hydrogen bond interaction between pyridine and dual silanols is very weak.

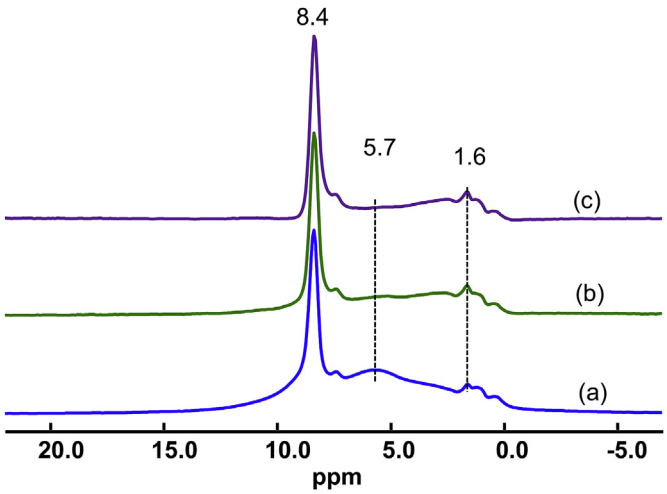

Fig. 7. ^{1}H spin-echo MAS NMR spectra of COE-4 zeolite with different time intervals: (a) 100 us, (b) 500 us, (c) 1000 us. The spinning rate of rotor is 10 kHz.

4. Conclusions

Interlayer expansion of RUB-36 with DCDMS leads to a new microporous material COE-4 which contains dual silanols with larger pore sizes. Multinuclear solid-state NMR techniques have been used to investigate the structure and porosity of COE-4. After interlayer expansion, the layer space of COE-4 is enlarged by 2.6 Å compared with that of RUB-37, indicating that pore sizes between the layers are

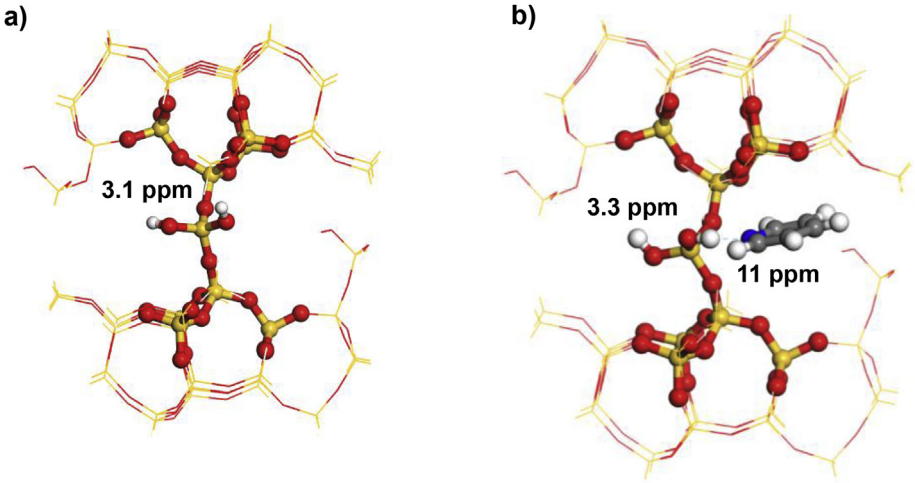

Fig. 6. Optimized cluster models of COE-4 before (a) and after (b) pyridine adsorption. The calculated ^{1}H chemical shifts of dual silanols are denoted.

enlarged from 8-MR to 10-MR pores after insertion of silicon pillar. HP ^{129}Xe NMR results demonstrate that Xe atoms can be adsorbed in the homogeneously formed 10-MR channels of COE-4 but can't enter the 8-MR pore of RUB-37. The interaction between Xe and 10-MR channel wall in COE-4 is stronger than ZSM-5 though they have similar pore size. ^{1}H MAS NMR results combined with theoretical calculations indicate that the signal of dual silanol groups appears at 3.3 ppm with an appreciable concentration of 2.2 mmol/g. After introduction of pyridine-d_5, the hydrogen bond interaction between pyridine and dual silanol is very weak and adsorbed pyridine may experience exchange with the other Si–OH of dual silanol groups. The approaches implemented in this work have been proved to be useful in study of the interlayer expanded zeolites.

Acknowledgements

We thank the supports of the National Natural Science Foundation of China (Nos. 21603022, 21872017, 91545104), LiaoNing Revitalization Talents Program (XLYC1807227), the Fundamental Research Funds for the Central Universities in China (No. DUT16RC (3) 002, DUT17TD04), the Supercomputing Center of Dalian University of Technology.

Appendix A. Supplementary data

Supplementary data to this article can be found online at https://doi.org/10.1016/j.micromeso.2019.06.017.

References

[1] M.E. Davis, Chem. Mater. 26 (2014) 239–245.
[2] C. Martínez, A. Corma, Coord. Chem. Rev. 255 (2011) 1558–1580.
[3] J. Li, A. Corma, J. Yu, Chem. Soc. Rev. 44 (2015) 7112–7127.
[4] C.S. Cundy, P.A. Cox, Microporous Mesoporous Mater. 82 (2005) 1–78.
[5] X. Meng, F.-S. Xiao, Chem. Rev. 114 (2014) 1521–1543.
[6] W.J. Roth, J. Čejka, Catal. Sci. Technol. 1 (2011) 43–53.
[7] W.J. Roth, P. Nachtigall, R.E. Morris, J. Čejka, Chem. Rev. 114 (2014) 4807–4837.
[8] B. Marler, H. Gies, Eur. J. Mineral. 24 (2012) 405–428.
[9] L. Xu, J. Sun, Adv. Energy. Mater. 6 (2016) 1600441.
[10] E. Verheyen, L. Joos, K. Van Havenbergh, E. Breynaert, N. Kasian, E. Gobechiya, K. Houthoofd, C. Martineau, M. Hinterstein, F. Taulelle, V. Van Speybroeck, M. Waroquier, S. Bals, G. Van Tendeloo, C.E.A. Kirschhock, J.A. Martens, Nat. Mater. 11 (2012) 1059–1064.
[11] W.J. Roth, P. Nachtigall, R.E. Morris, P.S. Wheatley, V.R. Seymour, S.E. Ashbrook, P. Chlubná, L. Grajciar, M. Položij, A. Zukal, O. Shvets, J. Čejka, Nat. Chem. 5 (2013) 628–633.
[12] P. Eliášová, M. Opanasenko, P.S. Wheatley, M. Shamzhy, M. Mazur, P. Nachtigall, W.J. Roth, R.E. Morris, J. Čejka, Chem. Soc. Rev. 44 (2015) 7177–7206.
[13] Z.C. Zhao, W.P. Zhang, Acta Phys. - Chim. Sin. 32 (2016) 2475–2487.
[14] P. Wu, J. Ruan, L. Wang, L. Wu, Y. Wang, Y. Liu, W. Fan, M. He, O. Terasaki, T. Tatsumi, J. Am. Chem. Soc. 130 (2008) 8178–8187.
[15] F.-S. Xiao, B. Xie, H.Y. Zhang, L. Wang, X.J. Meng, W.P. Zhang, X.H. Bao, B. Yilmaz, U. Müller, H. Gies, H. Imai, T. Tatsumi, D. De Vos, ChemCatChem 3 (2011) 1442–1446.
[16] H. Gies, M. Feyen, T. De Baerdemaeker, D.E. De Vos, B. Yilmaz, U. Müller, X. Meng, F.-S. Xiao, W. Zhang, T. Yokoi, T. Tatsumi, X. Bao, Microporous Mesoporous Mater. 222 (2016) 235–240.
[17] H. Gies, U. Müller, B. Yilmaz, T. Tatsumi, B. Xie, F.-S. Xiao, X.H. Bao, W.P. Zhang, D. De Vos, Chem. Mater. 23 (2011) 2545–2554.
[18] H. Gies, U. Müller, B. Yilmaz, M. Feyen, T. Tatsumi, H. Imai, H. Zhang, B. Xie, F.-S. Xiao, X. Bao, W. Zhang, T.D. Baerdemaeker, D. De Vos, Chem. Mater. 24 (2012) 1536–1545.
[19] B. Yilmaz, U. Müller, M. Feyen, H. Zhang, F.-S. Xiao, B.T. De, B. Tijsebaert, P. Jacobs, V.D. De, W. Zhang, X. Bao, H. Imai, T. Tatsumi, H. Gies, Chem. Commun. 48 (2012) 11549–11551.
[20] B. Tijsebaert, M. Henry, H. Gies, F.-S. Xiao, W. Zhang, X. Bao, H. Imai, T. Tatsumi, U. Müller, B. Yilmaz, J. Catal. 282 (2011) 47–53.
[21] B. Yilmaz, U. Müller, T. De Baerdemaeker, H. Gies, F.S. Xiao, T. Tatsumi, X. Bao, W. Zhang, D. De Vos, Metal-bridged Pillared Silicate Compounds and Process for Their Production, US Patent 2012/0004332, 2011.
[22] T. De Baerdemaeker, W. Vandebroeck, H. Gies, B. Yilmaz, U. Müller, M. Feyen, D. De Vos, Catal. Today 235 (2014) 169–175.
[23] T. De Baerdemaeker, H. Gies, B. Yilmaz, U. Mueller, M. Feyen, F.-S. Xiao, W. Zhang, T. Yokoi, X. Bao, D.E. De Vos, J. Mater. Chem. A 2 (2014) 9709–9717.
[24] J.F. Ruan, P. Wu, B. Slater, Z.L. Zhao, L.L. Wu, O. Terasaki, Chem. Mater. 21 (2009) 2904–2911.
[25] M.V. Opanasenko, W.J. Roth, J. Čejka, Catal. Sci. Technol. 6 (2016) 2467–2484.
[26] V.V. Terskikh, I.L. Moudrakovski, S.R. Breeze, S. Lang, C.I. Ratcliffe, J.A. Ripmeester, A. Sayari, Langmuir 18 (2002) 5653–5656.
[27] W. Zhang, C.I. Ratcliffe, I.L. Moudrakovski, C.-Y. Mou, J.A. Ripmeester, Anal. Chem. 77 (2005) 3379–3382.
[28] P. Sozzani, S. Bracco, A. Comotti, Chapter 9 Porous Materials Explored by Hyperpolarized Xenon NMR, Hyperpolarized Xenon-129 Magnetic Resonance: Concepts, Production, Techniques and Applications, The Royal Society of Chemistry2015, pp. 164-184.
[29] A. Comotti, S. Bracco, P. Valsesia, L. Ferretti, P. Sozzani, J. Am. Chem. Soc. 129 (2007) 8566–8576.
[30] L.-Q. Wang, D. Wang, J. Liu, G.J. Exarhos, S. Pawsey, I. Moudrakovski, J. Phys. Chem. C 113 (2009) 6577–6583.
[31] D.A. Barskiy, A.M. Coffey, P. Nikolaou, D.M. Mikhaylov, B.M. Goodson, R.T. Branca, G.J. Lu, M.G. Shapiro, V.-V. Telkki, V.V. Zhivonitko, I.V. Koptyug, O.G. Salnikov, K.V. Kovtunov, V.I. Bukhtiyarov, M.S. Rosen, M.J. Barlow, S. Safavi, I.P. Hall, L. Schröder, E.Y. Chekmenev, Chem. Eur. J. 23 (2017) 725–751.
[32] E. Weiland, M.-A. Springuel-Huet, A. Nossov, A. Gédéon, Microporous Mesoporous Mater. 225 (2016) 41–65.
[33] T. Meersmann, J.W. Logan, R. Simonutti, S. Caldarelli, A. Comotti, P. Sozzani, L.G. Kaiser, A. Pines, J. Phys. Chem. A 104 (2000) 11665–11670.
[34] S. Xu, W. Zhang, X. Liu, X. Han, X. Bao, J. Am. Chem. Soc. 131 (2009) 13722–13727.
[35] W. Zhang, S. Xu, X. Han, X. Bao, Chem. Soc. Rev. 41 (2012) 192–210.
[36] Z. Zhao, W. Zhang, P. Ren, X. Han, U. Müller, B. Yilmaz, M. Feyen, H. Gies, F.-S. Xiao, D. De Vos, T. Tatsumi, X. Bao, Chem. Mater. 25 (2013) 840–847.
[37] M. Müller, G. Harvey, R. Prins, Microporous Mesoporous Mater. 34 (2000) 281–290.
[38] D. Massiot, F. Fayon, M. Capron, I. King, S. Le Calvé, B. Alonso, J.-O. Durand, B. Bujoli, Z. Gan, G. Hoatson, Magn. Reson. Chem. 40 (2002) 70–76.
[39] C. Baerlocher, L.B. McCusker, Database of Zeolite Structures, http://www.iza-structure.org/databases/.
[40] J.P. Perdew, Phys. Rev. B 33 (1986) 8822–8824.
[41] Dmol3, Accelrys Inc, San Diego, CA, 2000.
[42] M. Frisch, G. Trucks, H. Schlegel, G. Scuseria, M. Robb, J. Cheeseman, G. Scalmani, V. Barone, B. Mennucci, G. Petersson, Inc., Wallingford, CT, 2009.
[43] A.D. Becke, J. Chem. Phys. 98 (1993) 5648–5652.
[44] N. Godbout, D.R. Salahub, J. Andzelm, E. Wimmer, Can. J. Chem. 70 (1992) 560–571.
[45] S. Komulainen, J. Roukala, Vladimir V. Zhivonitko, M.A. Javed, L. Chen, D. Holden, T. Hasell, A. Cooper, P. Lantto, V.-V. Telkki, Chem. Sci. 8 (2017) 5721–5727.
[46] J. Roukala, J. Zhu, C. Giri, K. Rissanen, P. Lantto, V.-V. Telkki, J. Am. Chem. Soc. 137 (2015) 2464–2467.
[47] S.F. Boys, F. Bernardi, Mol. Phys. 19 (1970) 553–566.
[48] X. Solans-Monfort, M. Sodupe, V. Branchadell, J. Sauer, R. Orlando, P. Ugliengo, J. Phys. Chem. B 109 (2005) 3539–3545.
[49] Y. Li, W. Guo, S. Yuan, W. Fan, J. Wang, H. Jiao, J. Mol. Struc.-THEOCHEM 916 (2009) 53–60.
[50] H. Li, J. Wang, D. Zhou, D. Tian, C. Shi, U. Müller, M. Feyen, H. Gies, F.-S. Xiao, D. De Vos, Microporous Mesoporous Mater. 218 (2015) 160–166.
[51] L.W. Chung, W.M. Sameera, R. Ramozzi, A.J. Page, M. Hatanaka, G.P. Petrova, T.V. Harris, X. Li, Z. Ke, F. Liu, H.B. Li, L. Ding, K. Morokuma, Chem. Rev. 115 (2015) 5678–5796.
[52] S. Grimme, J. Antony, S. Ehrlich, H. Krieg, J. Chem. Phys. 132 (2010) 154104.
[53] S. Grimme, S. Ehrlich, L. Goerigk, J. Comput. Chem. 32 (2011) 1456–1465.
[54] J. Klinowski, Chem. Rev. 91 (1991) 1459–1479.
[55] G. Engelhardt, H. Jancke, E. Lippmaa, A. Samoson, J. Organomet. Chem. 210 (1981) 295–301.
[56] I.L. Moudrakovski, V.V. Terskikh, C.I. Ratcliffe, J.A. Ripmeester, L.-Q. Wang, Y. Shin, G.J. Exarhos, J. Phys. Chem. B 106 (2002) 5938–5946.
[57] A. Nossov, E. Haddad, F. Guenneau, A. Gédéon, Phys. Chem. Chem. Phys. 5 (2003) 4473–4478.
[58] J. Fraissard, Chapter 1 Xenon as a Probe Atom: Introduction, Characteristics, Investigation of Microporous Solids, Hyperpolarized Xenon-129 Magnetic Resonance: Concepts, Production, Techniques and Applications, The Royal Society of Chemistry2015, pp. 1-15.
[59] Y. Liu, W. Zhang, S. Xie, L. Xu, X. Han, X. Bao, J. Phys. Chem. B 112 (2008) 1226–1231.
[60] M. Hanni, P. Lantto, J. Vaara, Phys. Chem. Chem. Phys. 11 (2009) 2485–2496.
[61] A. Zheng, H. Zhang, L. Chen, Y. Yue, C. Ye, F. Deng, J. Phys. Chem. B 111 (2007) 3085–3089.
[62] A. Zheng, S. Li, F. Deng, Solid-state NMR characterization of acidity of solid catalysts, in: G.A. Webb (Ed.), Modern Magnetic Resonance, Springer International Publishing, Cham, 2017, pp. 1–23.
[63] M. Hunger, Catal. Rev. Sci. Eng. 39 (1997) 345–393.